J. Fluid Mech. (1979), *vol.* 93, *part* 4, *pp.* 747–765
Printed in Great Britain

The unsteady quasi-vortex-lattice method with applications to animal propulsion

By C. E. LAN
Department of Aerospace Engineering, University of Kansas

(Received 1 February 1978 and in revised form 3 November 1978)

In the early theoretical study of aquatic animal propulsion either the two-dimensional theory or the large aspect-ratio theory has been generally used. Only recently has the unsteady lifting-surface theory with the continuous loading approach been applied to the study of this problem by Chopra & Kambe (1977). Since it is well known that the continuous loading approach is difficult to extend to general configurations, a new quasi-continuous loading method, applicable to general configurations and yet accurate enough for practical applications, is developed in this paper. The method is an extension of the steady version of Lan (1974) and is particularly suitable for predicting the unsteady lead-edge suction during harmonic motion.

The method is applied to the calculation of the propulsive efficiency and thrust for some swept and rectangular planforms by varying the phase angles between the pitching and heaving motions. It is found that with the pitching axis passing through the trailing edge of the root chord and the reduced frequency k equal to 0·75 the rectangular planform is quite sensitive in performance to the phase angles and may produce drag instead of thrust. These characteristics are not shared by the swept planforms simulating the lunate tails. In addition, when the pitching leads the heaving motion by 90°, the phase angle for nearly maximum efficiency, the planform inclination caused by pitching contributes to the propulsive thrust over a large portion of the swept planform, while, for the rectangular planform, only drag is produced from the planform normal force at $k = 0·75$. It is also found that the maximum thrust is not produced with maximum efficiency for all planforms considered. The theory is then applied to the study of dragonfly aerodynamics. It is shown that the aerodynamically interacting tandem wings of the dragonfly can produce high thrust with high efficiency if the pitching is in advance of the flapping and the hindwing leads the forewing with some optimum phase angle. The responsible mechanism allows the hindwing to extract wake energy from the forewing.

1. Introduction

In studying aquatic animal propulsion with the carangiform mode, Lighthill (1970) presented an unsteady two-dimensional aerofoil theory and showed that, for high thrust and high efficiency, the pitching axis should be near the trailing edge in a coupled heaving and pitching (or side-slipping and yawing) motion. The pitching was assumed to lead the heaving by 90°. Chopra (1974) extended Lighthill's investigation by using the large aspect-ratio theory for finite wings. Earlier, Bennett (1970) had also used the large aspect-ratio theory to study ornithopter aerodynamics. In a recent paper, Chopra & Kambe (1977) used Davies' lifting-surface method (1963) to investigate the hydromechanics of various planform shapes. They found that a curved leading edge, as on lunate tails, gives a reduced thrust contribution from the leading-edge suction for the same total thrust. However, moderate to high sweep angles suffer low propulsive efficiency at a given reduced frequency and feathering parameter, although more thrust can be produced with swept planforms. The feathering parameter, to be defined more precisely later, may be defined as the ratio of normal-velocity amplitude on the planform produced by pitching to that by heaving. The numerical study of Chopra & Kambe was carried out only with one phase angle between pitching and heaving. Apparently, the advantages of the lunate tails, which generally have high sweep angles, warrant further investigation in the hydrodynamical sense.

It should be noted that Davies' method is based on the kernel-function method in unsteady lifting-surface theory and is more difficult to extend for general configurations. In addition, the prediction of the unsteady leading-edge suction in the kernel-function method may very much depend on the number and arrangement of the collocation points in the solution of the integral equation, as evidenced in the study of the steady lifting-surface solutions by Lan & Lamar (1977). In Chopra & Kambe's study, the convergence of the predicted mean leading-edge suction with respect to the number and arrangement of the collocation points has not been demonstrated. On the other hand, the unsteady lifting-surface equation can also be solved by the doublet lattice method (DLM), which was developed by Albano & Rodden (1969) and has since been extended by many others. Although the DLM can be applied to quite general configurations, in its present form the unsteady leading-edge suction cannot be predicted accurately (see Kálmán, Giesing & Rodden 1970).

In this paper, a quasi-continuous method called the unsteady quasi-vortex-lattice method (unsteady QVLM) will be presented. The method is an extension of the steady QVLM of Lan (1974) and can be easily applied to general configurations with good accuracy. The predicted mean leading-edge thrust will be shown to be quite stable with respect to the number and arrangement of the collocation points. The method is then applied to show the importance of the phase angles between pitching and heaving to the performance of different planform shapes, thus shedding some light on the advantages of the lunate tails. The aerodynamic interaction between the flapping forewing and hindwing of the dragonfly will also be examined.

2. Mathematical formulation

It is assumed that the wings under consideration are situated on the x, y plane with the positive x axis lying along the root chord and pointing downstream, and the positive y axis pointing to the right, as shown in figure 1. The initial formulation will be based on the linear compressible flow theory, with the detail developed only for incompressible flow for applications to animal propulsion.

For a wing in heaving motion with displacement $\bar{h}(y, t)$ and in pitching with angular displacement $\bar{\alpha}(y, t)$ about $x = x_a$, the total vertical displacement $z(x, y, t)$ is given by

$$z(x, y, t) = -\bar{h}(y, t) - \bar{\alpha}(y, t)(x - x_a). \tag{2.1}$$

Mathematically, $\bar{h} - \bar{\alpha} x_a$ in (2.1) may be replaced by a new parameter independent of x.

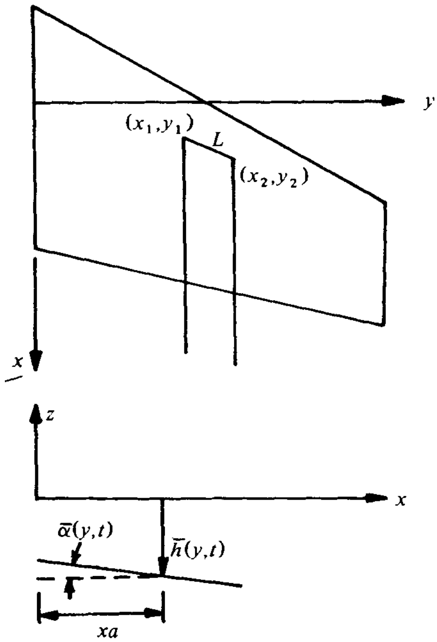

FIGURE 1. Definition of co-ordinate system.

However, the expression given by (2.1) is retained here for numerical convenience. It follows that the non-dimensional normal velocity on the wing is

$$\bar{w}(x, y, t) = \frac{1}{V}\frac{\partial z}{\partial t} + \frac{\partial z}{\partial x} = -\frac{1}{V}\dot{\bar{h}} - \bar{\alpha} - \frac{1}{V}\dot{\bar{\alpha}}(x - x_a), \tag{2.2}$$

where V is the freestream velocity. Assuming the harmonic time variation such that $\bar{w}(x,y,t) = \mathrm{Re}\,[w(x,y)\exp(i\omega t)]$, etc., (2.2) becomes

$$w(x,y) = -i\frac{k}{b_r}h(y) - \alpha(y)\exp[i(\phi_{\mathrm{ph}} - \pi)] - i\frac{k}{b_r}\alpha(y)\exp[i(\phi_{\mathrm{ph}} - \pi)](x - x_a), \tag{2.3}$$

where $k = \omega b_r / V$ is the reduced frequency and b_r is the reference length. The phase angle ϕ_{ph} of the pitching motion is relative to the heaving motion as illustrated in figure 2. Equation (2.3) can be reduced to the expression used by Lighthill (1970) by setting $\phi_{\mathrm{ph}} = \frac{1}{2}\pi$ and to that used by Wu (1971) by putting $x_a = 0$. The normal velocity given by (2.3) can be cancelled on the wing (i.e. satisfying the wing flow tangency condition) by the use of oscillating doublets. According to Richardson (1955), the non-dimensional velocity potential for doublets in an unsteady subsonic flow with Mach number M below the transonic range is given by

$$\bar{\phi}(x, y, z, t) = \frac{1}{8\pi}\iint_S \frac{\partial}{\partial \xi}\int_{(-x_0 + MR)/\beta^2}^{\infty} \Delta\bar{C}_p\left(\xi, \eta, t - \frac{\tau_1 + x_0}{V}\right)\frac{1}{r}\,d\tau_1\,d\xi\,d\eta, \tag{2.4}$$

where S is the wing area, $\Delta\bar{C}_p$ the non-dimensional lifting pressure, $\beta^2 = 1 - M^2$, $x_0 = x - \xi$, $y_0 = y - \eta$, $z_0 = z - \zeta$, (ξ, η, ζ) the co-ordinates of an elemental doublet and

$$r = (\tau_1^2 + y_0^2 + z_0^2)^{\frac{1}{2}}, \tag{2.5}$$

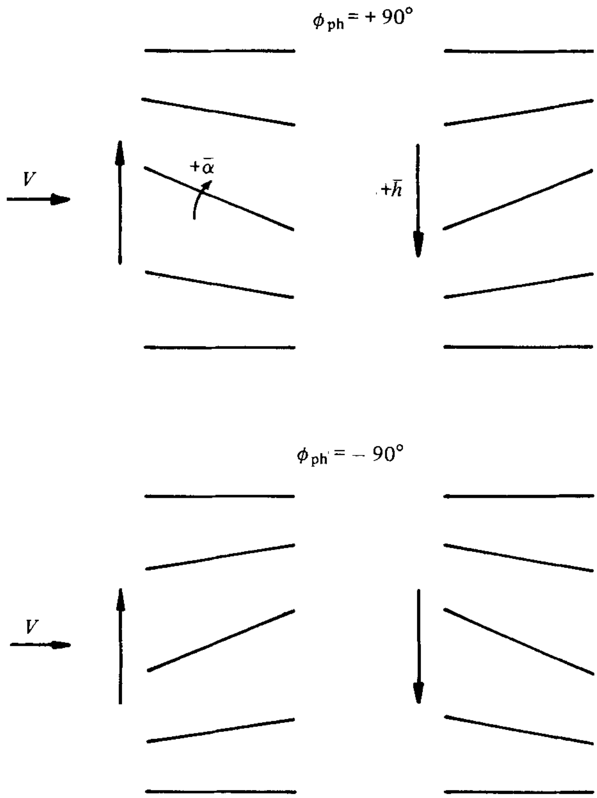

FIGURE 2. Illustration of phase angle of pitching relative to heaving, based on the following relations: $\bar{h} = h\cos\omega t$, $\bar{\alpha} = \alpha\cos(\omega t + \phi_{ph} - \pi)$.

$$R^2 = x_0^2 + \beta^2(y_0^2 + z_0^2). \tag{2.6}$$

If the harmonic time variation is introduced, then

$$\bar{\phi}(x, y, z, t) = \phi(x, y, z)\exp(i\omega t) \tag{2.7}$$

and

$$\Delta\bar{C}_p\left(\xi, \eta, t - \frac{\tau_1 + x_0}{V}\right) = \Delta C_p(\xi, \eta)\exp(i\omega t)\exp[-i\omega(\tau_1 + x_0)/V]. \tag{2.8}$$

Hence (2.4) is reduced to

$$\phi(x, y, z) = \frac{1}{8\pi}\iint_s \Delta C_p(\xi, \eta)\frac{\partial}{\partial\zeta}\int_{(-x_0+MR)/\beta^2 r}^{\infty} \frac{1}{r}\exp[-i\omega(\tau_1 + x_0)/V]\,d\tau_1\,d\xi\,d\eta. \tag{2.9}$$

By carrying out the differentiation of the integral in (2.9) first and then integrating by parts, (2.9) can be simplified to

$$\phi(x, y, z) = \frac{1}{8\pi}\iint_s \Delta C_p(\xi, \eta)\left\{\left(\frac{1}{r_1^2} + \frac{x_0}{Rr_1^2}\right) z_0 \exp[-i\omega(u_1 r_1 + x_0)/V] - i\frac{\omega}{V}\frac{z_0}{r_1}\exp[-i\omega x_0/V]\int_{u_1}^{\infty}\left[1 - \frac{\lambda}{(1+\lambda^2)^{\frac{1}{2}}}\right]\exp[-i\omega r_1\lambda/V]\,d\lambda\right\} d\xi\,d\eta, \tag{2.10}$$

where

$$u_1 r_1 = (-x_0 + MR)/\beta^2, \quad r_1 = (y_0^2 + z_0^2)^{\frac{1}{2}}. \tag{2.11}$$

Equation (2.10) is a convenient form in that the familiar steady expression is immediately recovered when $\omega = 0$.

From here on, the development of the formulation will be restricted to incompressible flow, so that $M = 0$ and $\beta = 1{\cdot}0$. To satisfy the wing boundary condition (2.3), the normal velocity $w = \partial\phi/\partial z$ must be obtained. For this purpose, (2.10) will be approximated through the following discretization. It is assumed that ΔC_p is stepwise constant in the spanwise direction and continuous in the chordwise direction. The resulting chordwise integral will be reduced to finite sums through the midpoint trapezoidal rule according to the QVLM procedure of Lan (1974). For swept planforms, it is more convenient to assume ΔC_p to be stepwise constant in the direction of constant per cent chord lines. Therefore, the planform will now be divided into strips in which ΔC_p is taken to be constant along the straight line L joining (x_1, y_1) and (x_2, y_2), where the point with subscript 1 is on the left side of a given strip and 2 is on the right side; see figure 1. By factoring ΔC_p out of the spanwise integral, the resulting integrand in the spanwise integration can be integrated by parts. For this purpose, let

$$x_0 = x - \xi = x - x_1 - \tau(x_2 - x_1) \tag{2.12}$$

and

$$y_0 = y - \eta = y - y_1 - \tau(y_2 - y_1). \tag{2.13}$$

The straight line L is now defined by (0, 1) in τ. If ϕ_1 is defined to be

$$\phi_1(x,y,z) = \frac{1}{8\pi}\int_L \left(\frac{1}{r_1^2} + \frac{x_0}{Rr_1^2}\right) z_0\, d\eta \tag{2.14}$$

then (2.14) can be integrated to give

$$\phi_1(x, y, z) = \frac{1}{8\pi} F \Big|_L \tag{2.15}$$

where

$$F = -\tan^{-1}\frac{Qv - (x_2 - x_1) z^2}{z(y_2 - y_1)(A\tau^2 + B\tau + C)^{\frac{1}{2}}} + \tan^{-1}\frac{2a\tau + b}{2(y_2 - y_1) z}, \tag{2.16}$$

$$\begin{aligned}
v &= (y_2 - y_1)\tau - (y - y_1) = \eta - y,\\
a &= (y_2 - y_1)^2, \quad b = -2(y - y_1)(y_2 - y_1);\\
Q &= (x_2 - x_1)(y - y_1) - (x - x_1)(y_2 - y_1),\\
A &= (x_2 - x_1)^2 + (y_2 - y_1)^2,\\
B &= -2[(x - x_1)(x_2 - x_1) + (y - y_1)(y_2 - y_1)],\\
C &= (x - x_1)^2 + (y - y_1)^2 + z^2.
\end{aligned} \tag{2.17}$$

A similar procedure can be applied to the second integral (to be denoted by ϕ_2) in (2.10). Let

$$I(x,y,z,\xi,\eta) = r_1 \int_{u_1}^{\infty} \left[1 - \frac{\lambda}{(1+\lambda^2)^{\frac{1}{2}}}\right] \exp\left[-i\omega(r_1\lambda + x_0)/V\right] d\lambda \tag{2.18a}$$

$$= \int_{u_1 r_1}^{\infty} \left[1 - \frac{\tau_1}{(\tau_1^2 + r_1^2)^{\frac{1}{2}}}\right] \exp\left[-i\omega(\tau_1 + x_0)/V\right] d\tau_1. \tag{2.18b}$$

It follows that

$$\phi_2(x, y, z) = -i\frac{\omega}{V}\frac{1}{8\pi}\left\{\tan^{-1}\frac{2a\tau + b}{2(y_2 - y_1) z} I \Big|_L - \int_L \tan^{-1}\frac{2a\tau + b}{2(y_2 - y_1) z}\frac{\partial I}{\partial \eta} d\eta\right\}. \tag{2.19}$$

Substituting (2.15) and (2.19) into (2.10), and differentiating with respect to z, the following is obtained:

$$\frac{\partial\phi}{\partial z}(x, y, z) = \Sigma \int_{x_l}^{x_t} \Delta C_p(\xi) \left(\frac{\partial\phi_1}{\partial z} + \frac{\partial\phi_2}{\partial z}\right) d\xi, \tag{2.20}$$

where Σ denotes the summation over all spanwise strips and x_l, x_t are the x co-ordinates of the leading and trailing edges, respectively, of the chord through the collocation (or control) points (to be specified later). The detailed expressions for $\partial\phi_1/\partial z$ and $\partial\phi_2/\partial z$ are given in appendix A. It should be remarked that the steady version of (2.20) can be shown to be the result for conventional horseshoe vortices derived by the Biot–Savart law.

With the transformation

$$\xi = x_l + \tfrac{1}{2}c(1 - \cos\theta) \tag{2.21}$$

(2.20) becomes

$$\frac{\partial\phi}{\partial z}(x, y, z) = \Sigma \frac{c}{2} \int_0^{\pi} \Delta C_p(\theta) \sin\theta \left(\frac{\partial\phi_1}{\partial z} + \frac{\partial\phi_2}{\partial z}\right) d\theta. \tag{2.22}$$

Note that $\sin\theta$ cancels the square-root singularities of ΔC_p at the leading and trailing edges. Therefore, the integral in (2.22) can be reduced to a finite sum through the midpoint trapezoidal rule with excellent accuracy. Any Cauchy singularity in the chordwise integral (see appendix B) can be accounted for by choosing a special set of control points to be given later. Hence

$$\frac{\partial\phi}{\partial z}(x, y, z) = \Sigma \frac{c}{2} \frac{\pi}{N_c} \sum_{k=1}^{N_c} \Delta C_p(\theta_k) \sin\theta_k \left(\frac{\partial\phi_{1k}}{\partial z} + \frac{\partial\phi_{2k}}{\partial z}\right), \tag{2.23}$$

where N_c is the number of integration points and $\theta_k = (2k-1)\pi/(2N_c)$. Using (2.21), it can be determined that the chordwise locations of the 'bounded' element of the horseshoe vortices are given by

$$\xi_k = x_l + \tfrac{1}{2}c[1 - \cos(2k-1)\pi/2N_c], \quad k = 1, \ldots, N_c. \tag{2.24}$$

The x co-ordinates of endpoints of the bounded elements are given by

$$x_{1k} = \xi_{1k}, \quad x_{2k} = \xi_{2k}, \tag{2.25}$$

where ξ_{1k} and ξ_{2k} are with x_{l_1}, c_1 and x_{l_2}, c_2, respectively. According to Lan (1974), the control points at which (2.3) is to be satisfied must be chosen such that

$$x_i = x_l + \tfrac{1}{2}c[1 - \cos(i\pi/N_c)], \quad i = 1, \ldots, N_c, \tag{2.26}$$

and

$$y_j = \tfrac{1}{2}(\tfrac{1}{2}b)[1 - \cos(j\pi/(N_s+1))], \quad j = 1, \ldots, N_s, \tag{2.27}$$

where N_s is the number of spanwise strips. The spanwise division of the planform into strips is also based on the cosine distribution:

$$y_k = \tfrac{1}{2}(\tfrac{1}{2}b)[1 - \cos(2k-1)\pi/(N_s+1)], \quad k = 1, \ldots, (N_s+1). \tag{2.28}$$

Combining (2.3) and (2.20) and satisfying the boundary condition at the control points, a finite number of ΔC_p values can be computed. These ΔC_p values are then used to obtain the lift and pitching moment coefficients through integration (see Lan 1974).

The main interest here is the computation of the propulsive thrust and the propulsive efficiency during a cycle of the oscillation. The propulsive thrust consists of the difference of two components, the first being represented by the mean leading-edge thrust coefficient $\bar{C}_{Tl}$, and the second the lift vector component, $L\bar{\alpha}$. If the complex sectional lift coefficient is $c_l(y)$ at y, then the contribution of the latter to the propulsive thrust is

$$-qc\,\mathrm{Re}\,[c_l(y)\,e^{i\omega t}]\,\mathrm{Re}\,[\alpha(y)\,e^{i(\phi_{\mathrm{ph}}-\pi)}\,e^{i\omega t}]\,dy,$$

where Re means the real part and q the dynamic pressure. The mean value over one cycle is therefore

$$-qc\tfrac{1}{2}\{c_{l\mathrm{r}}(y)\,\mathrm{Re}\,[\alpha(y)\,e^{i(\phi_{\mathrm{ph}}-\pi)}]+c_{l\mathrm{i}}(y)\,\mathrm{Im}\,[\alpha(y)\,e^{i(\phi_{\mathrm{ph}}-\pi)}]\}\,dy,$$

where the subscripts r, i denote the real and imaginary parts, respectively. Hence, the mean total propulsive thrust is given by

$$\bar{T}=qSC_T=qS\left\{\bar{C}_{Tl}-\frac{1}{2S}\int_{-\frac{1}{2}b}^{\frac{1}{2}b}[c_{l\mathrm{r}}(y)\,\mathrm{Re}\,(\alpha\,e^{i(\phi_{\mathrm{ph}}-\pi)})+c_{l\mathrm{i}}(y)\,\mathrm{Im}\,(\alpha\,e^{i(\phi_{\mathrm{ph}}-\pi)})]\,c\,dy\right\}. \quad (2.29)$$

$\bar{C}_{Tl}$ is computed by following the procedure used in the QVLM and is formulated in appendix B.

To compute the efficiency, we note that the input power (I.P.) to sustain the oscillation is the negative of the power produced by the lift, $-L\dot{\bar{h}}$, and by the moment, $\mathscr{M}\dot{\bar{\alpha}}$. The negative sign for $L\dot{\bar{h}}$ comes from the assumption that $\bar{h}$ is positive downward, while L is positive upward. Hence

$$\begin{aligned}\mathrm{I.P.}=L\dot{\bar{h}}-\mathscr{M}\dot{\bar{\alpha}}&=q\int_{-\frac{1}{2}b}^{\frac{1}{2}b}\mathrm{Re}\,[c_l(y)\,e^{i\omega t}]\,\mathrm{Re}\,[i\omega h(y)\,e^{i\omega t}]\,c(y)\,dy\\&\quad-q\int_{-b/2}^{b/2}\mathrm{Re}\,[c_m(y)\,e^{i\omega t}]\,\mathrm{Re}\,[i\omega\alpha(y)\,e^{i(\phi_{\mathrm{ph}}-\pi)}\,e^{i\omega t}]\,c^2(y)\,dy.\end{aligned} \quad (2.30)$$

The mean value over one cycle of oscillation can be shown to be

$$\begin{aligned}\overline{\mathrm{I.P.}}=q\omega\int_{-\frac{1}{2}b}^{\frac{1}{2}b}\tfrac{1}{2}h(y)\,c_{l\mathrm{i}}(y)\,c(y)\,dy-q\omega\int_{-\frac{1}{2}b}^{\frac{1}{2}b}\tfrac{1}{2}[c_{m\mathrm{i}}(y)\,\mathrm{Re}\,(\alpha(y)\,e^{i(\phi_{\mathrm{ph}}-\pi)})\\-c_{m\mathrm{r}}(y)\,\mathrm{Im}\,(\alpha(y)\,e^{i(\phi_{\mathrm{ph}}-\pi)})]\,c^2(y)\,dy.\end{aligned} \quad (2.31)$$

It follows that the propulsive efficiency is given by

$$\eta=\bar{T}V/\overline{\mathrm{I.P.}} \quad (2.32)$$

3. Numerical results and discussion

The idea used in the preceding formulation has also been applied to two-dimensional cases in subsonic flow (Lan 1975); some three-dimensional results have been reported by Lan (1976). It was shown in the above two references that the calculation of the unsteady leading-edge suction by the present method is quite accurate in two-dimensional cases. In three-dimensional cases, the computed results for a rectangular wing with an aspect ratio (A) of 2·0 oscillating in its first bending mode have been compared with other results with good agreement.

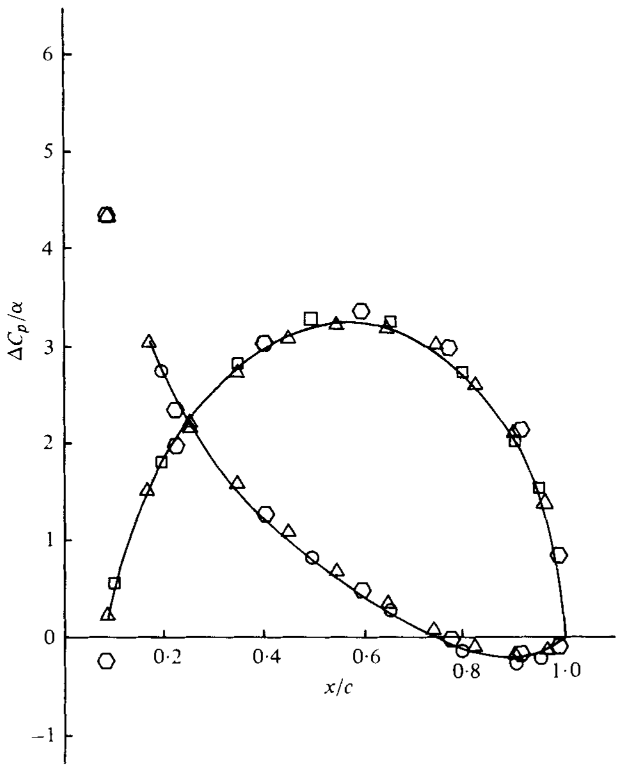

FIGURE 3. Comparison of predicted chordwise pressure distribution at mid-semispan on a circular wing in pitching with axis through centre at $M = 0$ and $k = 0{\cdot}8$ based on half chord at mid-semi-span. ——, analytic results by van Spiegel; ○, real part and, □, imaginary part by Laschka's method; △, DLM. All of above results taken from Stahl *et al.* (1968). ⬡, present method.

To illustrate further the accuracy of the present formulation, the calculated pressure distribution along the chord at mid-semispan of a circular wing in pitching oscillation at incompressible flow is compared with other theoretical methods in figure 3. The number of chordwise collocation points (N_c) is taken to be 8 and that of spanwise strips (N_s) on the half-wing is 7. It is seen that the present results are in good agreement with others.

Before the application to animal and insect propulsion can be investigated, the accuracy of the present method in predicting the propulsive thrust and efficiency must be established. Chopra & Kambe (1977) have presented some results for several planforms by a lifting-surface method. To avoid the effects of sweep and taper on the numerical accuracy, the rectangular wing of $A = 8{\cdot}0$ included in Chopra & Kambe's study is chosen for comparison. The results for $\phi_{\mathrm{ph}} = 90°$ are presented in figure 4; they are for different values of the feathering parameter ($\bar{\theta}$) defined as

$$\bar{\theta} = |\alpha|\, v/h\omega. \tag{3.1}$$

For $\bar{\theta} = 0$, only heaving motion exists. Figure 4(a) shows the good convergence characteristics of the present method for $\bar{\theta} = 0$. It is seen from figure 4(b) calculated

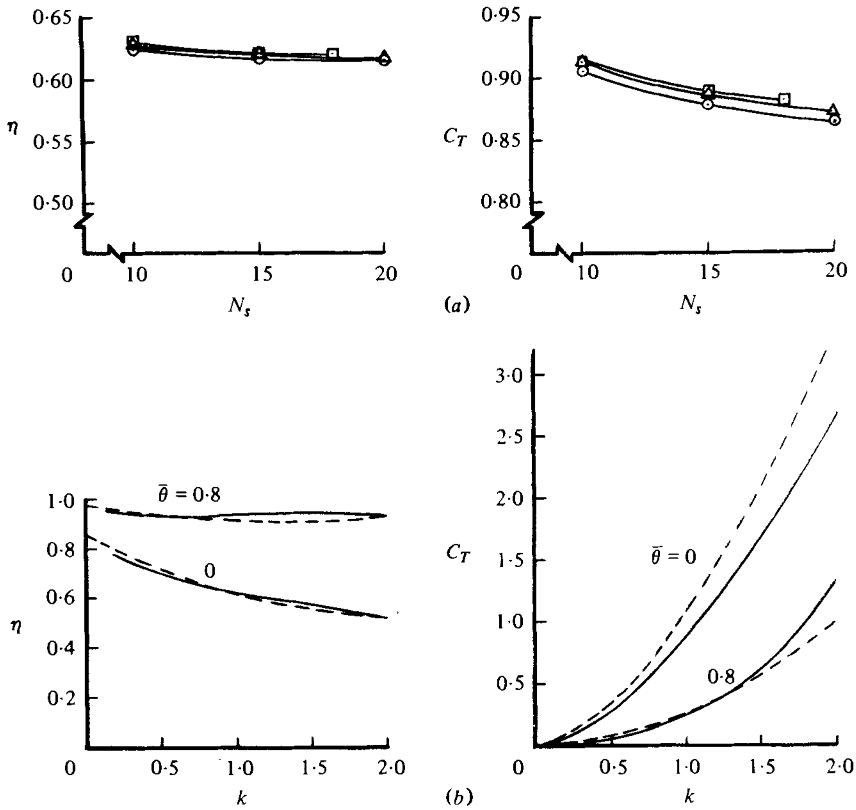

FIGURE 4. Rectangular wing of $A = 8{\cdot}0$ in pitching about $\frac{3}{4}$ chord line and in heaving; $h = c$ and $b_r = c$. (*a*) Convergence study for $\bar{\theta} = 0$ with —○— for $N_c = 3$, —△— $N_c = 4$ and —□— $N_c = 5$. (*b*) Comparison of present results (——) with Chopra & Kambe's (1977) (– – – –).

with $N_c \times N_s = 5 \times 13$ that the present results for propulsive efficiency agree quite well with Chopra & Kambe's. The agreement for the propulsive thrust is not as good, in particular at high reduced frequencies. The reason for the discrepancy is not known, since no exact solution is available for comparison.

In their investigation of lunate-tail swimming propulsion, Chopra & Kambe (1977) indicated numerically that a curved leading edge gives a reduced thrust contribution from the leading-edge suction for the same total thrust and the effect of leading-edge sweep is to reduce the propulsive efficiency. Examination of some existing fast swimming fish shows that the leading-edge sweeping angles of the lunate tails can range from 30° for the dolphin to 50° for the sailfish and up to 65° for the rainbow trout. Therefore, it is worthwhile to investigate further the sweep effect on the swimming performance of fish. For this purpose, a rectangular planform and an arrow wing are chosen. Both have the same aspect ratio of 7·0, which is typical for many fish. The arrow planform has a leading-edge sweep angle of 50°. The pitching axis is taken to pass through the trailing edge of the root chord. The results for $\bar{\theta} = 0{\cdot}8$ and $k = 0{\cdot}15$ and $0{\cdot}75$ are plotted against the phase angle ϕ_{ph} in figure 5. The reduced frequency is referred to half of the average chord. It is seen that both the rectangular and arrow planforms have comparable performance at the low

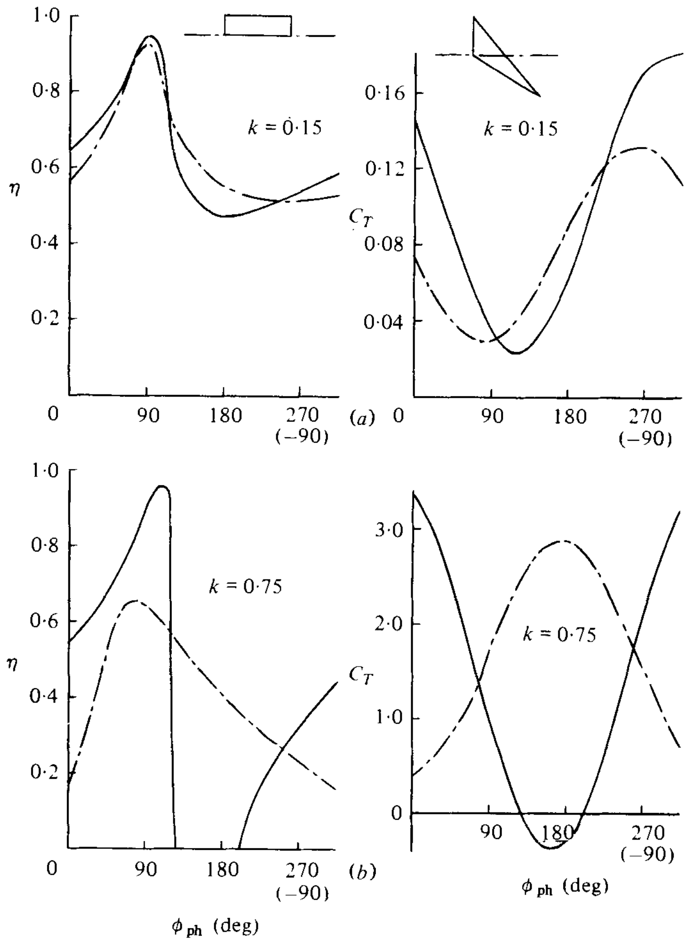

FIGURE 5. Comparison of propulsive performance for rectangular wing (——) and arrow wing (— – –) for $k = 0{\cdot}15$ and $0{\cdot}75$, heaving amplitude $h = 1$, and $\bar{\theta} = 0{\cdot}8$.

reduced frequency (for cruising). In fact, for $0 < \phi_{ph} < 90°$, the rectangular planform has higher η and C_T. A general observation of the results at $k = 0{\cdot}15$ is that, for high propulsive efficiency, the pitching motion must lead the heaving, with $\phi_{ph} \simeq 90°$. The resulting thrust is near the minimum. On the other hand, maximum thrust occurs with the pitching lagging the heaving. However, as shown in figure 6 for the resulting normal force (i.e. the side force for most fish) with $k = 0{\cdot}15$, the maximum thrust is associated with large side force which is not desirable as indicated by Lighthill (1970). The physical phenomenon involved can be explained by referring to figure 2, assuming that quasi-steady approximation is applicable. With $\bar{\theta} = 0{\cdot}8$, the normal velocity produced by heaving dominates. For $\phi_{ph} = 90°$, the heaving normal velocity is reduced by the normal velocity due to pitching. This decreases the loading and hence the necessary input power. The leading-edge thrust is also reduced. However, the planform normal force will produce a thrust component. For example, as the planform is moving up, a download is produced. When it is moving down, an upload is produced. Both situations will result in a thrust component from the normal force. The situation associated with $\phi_{ph} = -90°$ is just the opposite.

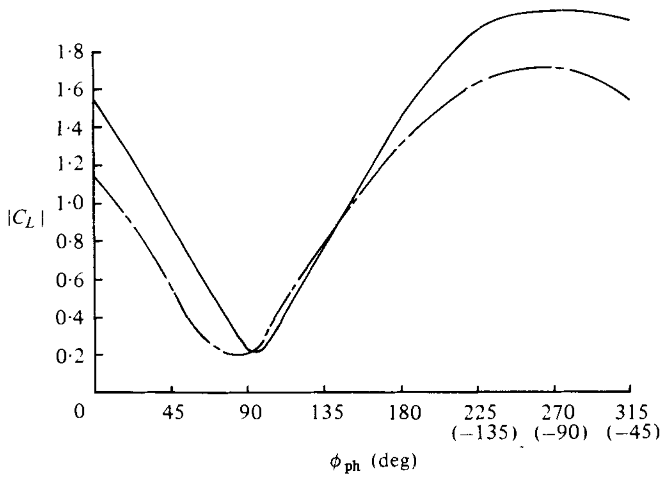

FIGURE 6. Comparison of the normal force coefficient on the rectangular wing (——) and arrow wing (— — —) for $k = 0{\cdot}15$, $h = 1$ and $\bar{\theta} = 0{\cdot}8$.

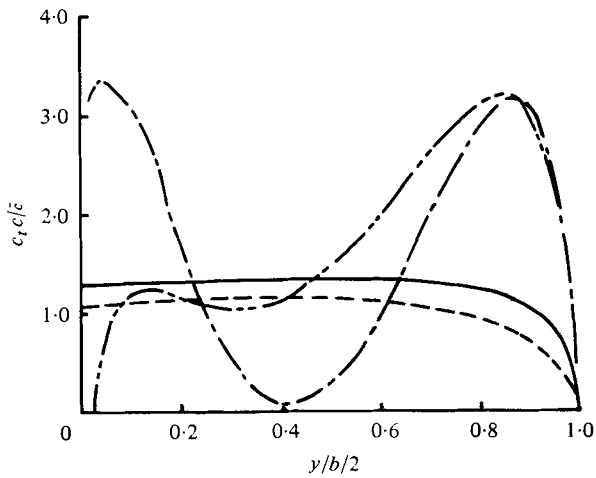

FIGURE 7. Sectional thrust distribution for $k = 0{\cdot}75$, $\bar{\theta} = 0{\cdot}8$, $h = 1$ and $\phi_{\text{ph}} = 90°$. Rectangular wing: ——, leading-edge suction only; - - - -, total. Arrow wing: — - — —, leading-edge suction only; — – – – —, total.

The normal velocity produced by heaving and pitching is additive and thus produces high loading and high leading-edge thrust which is reduced by the drag component of the normal force. Since high leading-edge thrust may lead to flow separation, negative ϕ_{ph} is always avoided in nature. As shown by Hertel (1966), $\phi_{\text{ph}} \simeq 72°$ for the rainbow trout and is 105° and 75° for sturgeon tail and fin, respectively.

Examination of the results for the reduced frequency of 0·75 in figure 5 shows that, for ϕ_{ph} in the range of 120° and 195°, the rectangular planform produces drag instead of thrust, while the arrow planform always produces thrust. The high sensitivity of the performance of the rectangular planform to the change in ϕ_{ph} may represent one of its disadvantages. In addition, the rectangular planform tends to produce its thrust completely from the leading-edge suction; while this is not true for the arrow planform.

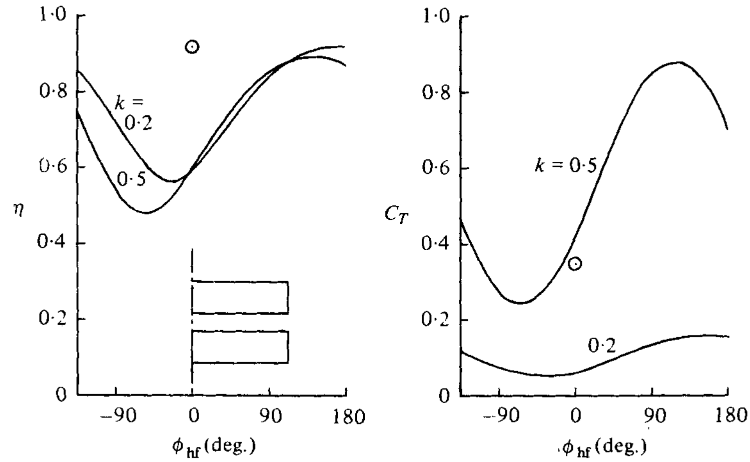

FIGURE 8. Propulsive performance of a tandem-wing configuration in pure flapping with wing gap equal to half chord. C_T is based on one wing area and k based on half chord. ⊙ for $k = 0{\cdot}5$ and fixed hindwing. ϕ_{hf} is the phase angle of hindwing motion relative to forewing.

This is illustrated in figure 7 for $\phi_{ph} = 90°$. For the arrow planform, the planform normal force contributes to the propulsive thrust over a large portion of the planform, except that near the root which is normally covered by the body, or by a much thicker section to reduce the flow separation. Additional calculations indicate that the characteristics of the thrust generation by the arrow planform remain similar with different pitching axis locations and are also similar for the delta planform. At low reduced frequencies, the planform normal force tends to produce propulsive thrust also for the rectangular planform. The situation is changed at a value of k greater than 0·5.

As shown above, the maximum propulsive thrust for any planform shape at a given reduced frequency is not produced with the maximum efficiency. To explore the possibility of high thrust produced at high efficiency, the dragonfly aerodynamics will be examined. The dragonflies were considered by Chadwick (1940) as among the swiftest and most skilful flyers. Their hindwings have been observed to flap always in advance of the forewings. To study the aerodynamics it is assumed that the motion is harmonic, although it is only periodic in nature. For simplicity, two rectangular planforms of aspect ratio 6 are placed in tandem with the gap between being a half-chord, and are used to generate most of the following results. In reality, the gap varies from more than one chord length at the tip to zero inboard of the mid-semispan. The thrust coefficient is referred to a single planform area. The pitching axes are assumed to be at the trailing edges of the planforms. The flapping amplitude is assumed to vary linearly from zero at the root to h_t at the tip, with h_t being unity. The pitching amplitude is assumed to take the form $\alpha_t \bar{y} \exp[i(\phi_{ph} - \pi)]$, where $\bar{y}$ is the spanwise fraction of the semispan. The feathering parameter $\bar{\theta}$ is defined by h_t and α_t. The results for pure flapping with $k = 0{\cdot}2$ and $0{\cdot}5$ are shown in figure 8. They illustrate the energy extraction by the hindwing from the wake of the forewing. Bosch (1972) (see also Laschka 1975) studied this problem in two dimensions with pure heaving and showed that the propulsive efficiency can be greatly increased if the hindwing is fixed. The present three-dimensional results at $k = 0{\cdot}5$ indicate that, although η is high if the

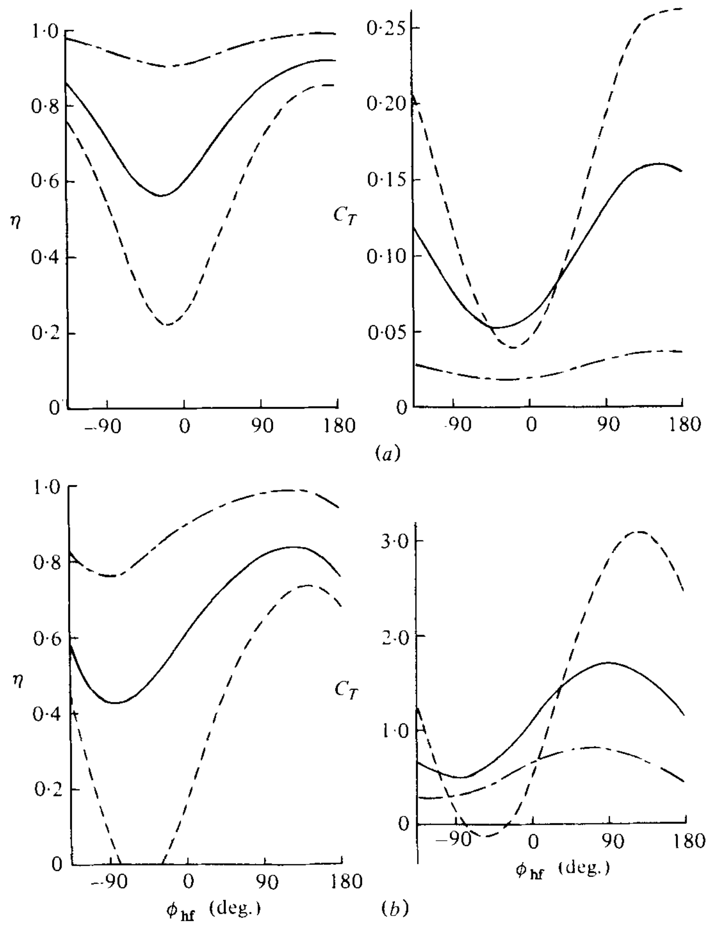

FIGURE 9. Comparison of propulsive performance of a tandem-wing configuration with wing gap equal to half chord. (*a*) $k = 0{\cdot}2$, (*b*) $k = 0{\cdot}75$. Linear variation of flapping and pitching amplitudes from zero at root. $\overline{\theta}$ defined with tip amplitudes. ——, $\overline{\theta} = 0$; — — —, $\overline{\theta} = 0{\cdot}8$, $\phi_{ph} = 90°$; – – – –, $\overline{\theta} = 0{\cdot}8$, $\phi_{ph} = -90°$.

hindwing is fixed, the resulting thrust would be low. It is advantageous to have both tandem wings oscillating, but with appropriate phase angle (ϕ_{hf}) between the two to produce both high thrust and high efficiency. The appropriate ϕ_{hf} is such that the hindwing must move in advance of the forewing. Note also that, as k is increased, the optimum ϕ_{hf} is decreased. This energy extraction concept has also been discussed theoretically by Sparenberg & Wiersma (1974) and is similar to the energy extraction from a wavy stream as discussed by Wu (1972).

Since in nature the motion is always in combined pitching and flapping, the results for $k = 0{\cdot}2$ and $0{\cdot}75$ and two different $\overline{\theta}$'s are shown in figure 9. It is seen that, for $k = 0{\cdot}2$ with ϕ_{ph} equal to 90° (i.e. pitching in advance of flapping), the efficiency is, in general, the best among the three and the thrust generated is the least. What is significant is that the maximum thrust can be generated with maximum efficiency if the hindwing flaps in advance of the forewing by 135° ~ 180°. With pitching lagging flapping ($\phi_{ph} = -90°$), its apparent high thrust is generated completely from the

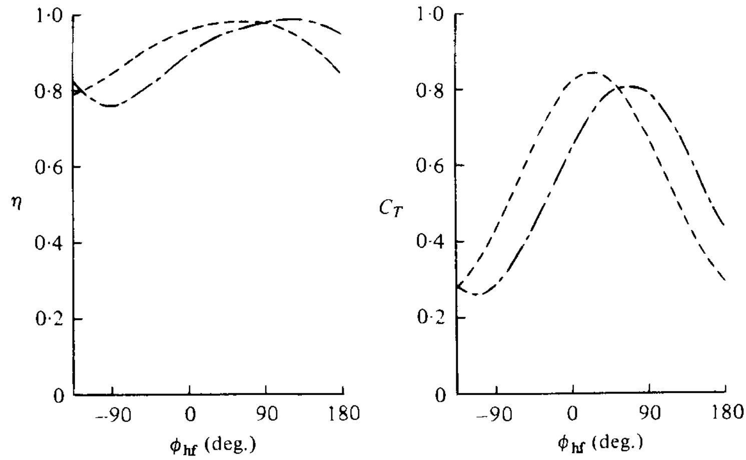

FIGURE 10. Comparison of propulsive performance of a tandem-wing configuration with different wing gaps. $\bar{\theta} = 0{\cdot}8$, $\phi_{ph} = 90°$ and $k = 0{\cdot}75$. ———, wing gap = half chord; – – – –, wing gap = one chord.

leading-edge suction, with the planform normal force producing only drag. For $\phi_{ph} = 90°$, the planform normal force produces the thrust. The relative trend for $k = 0{\cdot}75$ is quite similar to that at $k = 0{\cdot}2$, except that the optimum phase angle of hindwing motion relative to the forewing (ϕ_{hf}) has decreased. The optimum ϕ_{hf} appears to be different for maximum η ($\phi_{hf} \simeq 112°$ with $\phi_{ph} = 90°$) and C_T ($\phi_{hf} \simeq 67°$ with $\phi_{ph} = 90°$). The maximum efficiency for $k = 0{\cdot}75$ is about the same as for $k = 0{\cdot}2$ with $\phi_{ph} = 90°$. However, at this higher reduced frequency, η is considerably reduced for $\phi_{ph} = -90°$ and for the pure flapping case. If the wing gap is now increased to one chord length, the optimum ϕ_{hf} is further decreased, as shown in figure 10. For maximum η and C_T, the optimum $\phi_{hf} \simeq 67°$ and 22°, respectively. As mentioned earlier, the wing gap between the dragonfly tandem wings varies across the span. Therefore, as an approximation, the above results may be averaged to give the optimum $\phi_{hf} \simeq 90°$ and 45° for maximum η and C_T, respectively, at $k = 0{\cdot}75$. This result seems to agree qualitatively with the observation of a tethered insect (Pringle 1957). Therefore, it may be speculated that a tethered insect may flap its wings at higher frequencies than in normal flight just to generate more thrust at high efficiency.

The author is grateful to Dr William P. Rodden for constant encouragement during this research and for reading the manuscript. Thanks are also due to Jeffrey Miller for obtaining some of the numerical results and to Tze-Chuan Shu for plotting the results. This research was sponsored by the University of Kansas general research allocation no. 3896–5038.

Appendix A. Normal-velocity expressions for a unit oscillating horseshoe vortex

Differentiating (2.15) with respect to z in incompressible flow gives

$$\frac{\partial \phi_1}{\partial z} = \frac{1}{8\pi} \frac{\partial F}{\partial z}\bigg|_L = W_1, \tag{A 1}$$

where

$$W_1 = \left\{ -\frac{\eta - y}{(\eta-y)^2+z^2} + \frac{1}{[(x-\xi)^2+(\eta-y)^2+z^2]^{\frac{1}{2}}} \left[\frac{(\eta-y)(\xi-x)}{(\eta-y)^2+z^2} \right.\right.$$
$$\left.\left. + Q\,\frac{(\xi-x)(x_2-x_1)+(y_2-y_1)(\eta-y)}{Q^2+z^2[(x_2-x_1)^2+(y_2-y_1)^2]} \right] \right|_{(\xi,\,\eta)=(x_1,\,y_1)}^{(x_2,\,y_2)} \tag{A 2}$$

Similarly, differentiating (2.19) with respect to z gives

$$\frac{\partial \phi_2}{\partial z} = -i\frac{\omega}{V}\frac{1}{8\pi}\left\{ -\frac{y_2-y}{(y_2-y)^2+z^2} I_2 + \frac{y_1-y}{(y_1-y)^2+z^2} I_1 + \tan^{-1}\left(\frac{y_2-y}{z}\right)\frac{\partial I_2}{\partial z} \right.$$
$$\left. -\tan^{-1}\left(\frac{y_1-y}{z}\right)\frac{\partial I_1}{\partial z} + W_2 + W_3 \right\}, \tag{A 3}$$

$$W_2 = \int_0^1 \frac{\eta-y}{(\eta-y)^2+z^2}\frac{\partial I}{\partial \eta}(y_2-y_1)\,d\tau \tag{A 4}$$

and

$$W_3 = -\int_0^1 \tan^{-1}\frac{\eta-y}{z}\,\frac{\partial^2 I}{\partial z\,\partial \eta}(y_2-y_1)\,d\tau. \tag{A 5}$$

In (A 3), I_1 and I_2 are defined through (2.18) such that

$$I_1 = I(x, y, z, x_1, y_1) \tag{A 6}$$

and

$$I_2 = I(x, y, z, x_2, y_2).$$

Differentiating I with respect to z gives

$$\frac{\partial I}{\partial z} = z\int_{u_1 r_1}^{\infty} \frac{\tau_1\, e^{-i\omega(\tau_1+x_0)/V}}{(\tau_1^2+r_1^2)^{\frac{3}{2}}}\,d\tau_1. \tag{A 7}$$

Similarly, $\partial I/\partial \eta$ can be obtained as

$$\frac{\partial I}{\partial \eta} = \frac{\partial I}{\partial r_1}\frac{\partial r_1}{\partial \eta} + \frac{\partial I}{\partial x_0}\frac{\partial x_0}{\partial \eta} = -(y-\eta)\int_{u_1 r_1}^{\infty} \frac{\tau_1 \exp[-i\omega(\tau_1+x_0)/V]}{(\tau_1^2+r_1^2)^{\frac{3}{2}}}\,d\tau_1$$
$$+ i\frac{\omega}{V} I\frac{x_2-x_1}{y_2-y_1} - \left[1 - \frac{u_1}{(1+u_1^2)^{\frac{1}{2}}}\right]\frac{x_2-x_1}{y_2-y_1}. \tag{A 8}$$

Equation (A 8) can be used to find $\partial^2 I/\partial z\,\partial \eta$:

$$\frac{\partial^2 I}{\partial z\,\partial \eta} = \frac{z}{r_1}\frac{\partial}{\partial r_1}\left(\frac{\partial I}{\partial \eta}\right) = \frac{3(y-\eta)z}{r_1^2}\left[r_1^2 \int_{u_1 r_1}^{\infty} \frac{\tau_1 \exp[-i\omega(\tau_1+x_0)/V]}{(\tau_1^2+r_1^2)^{\frac{5}{2}}}\,d\tau_1 \right]$$
$$+ i\frac{\omega}{V}\frac{z}{r_1}\frac{\partial I}{\partial r_1}\frac{x_2-x_1}{y_2-y_1} + \frac{1}{(1+u_1^2)^{\frac{3}{2}}}\frac{x_2-x_1}{y_2-y_1}\left(\frac{x_0}{r_1^2}\right). \tag{A 9}$$

It should be noted that the above expressions will be automatically reduced to those for the steady horseshoe vortices by setting $\omega = 0$.

In (A 3)–(A 9), three are three types of integrals which must be evaluated numerically. One possible way is to approximate the function $\lambda/(1+\lambda^2)^{\frac{1}{2}}$ by the following expression due to Jordan (1976):

$$\frac{\lambda}{(1+\lambda^2)^{\frac{1}{2}}} \simeq 1-\sum_{n=1}^{10} a_n \exp(-c_n \lambda), \tag{A 10}$$

where a_n and c_n are constants obtained by Jordan. With (A 10), the integrals can be integrated exactly. These are discussed below.

$$(a)\ T_1 \equiv I = r_1 \exp(-i\omega x_0/V) \int_{u_1}^{\infty} [1-\lambda/(1+\lambda^2)^{\frac{1}{2}}] \exp(-i\omega r_1 \lambda/V)\, d\lambda. \tag{A 11}$$

Equation (A 11) can be directly evaluated after substitution of (A 10). If u_1 is negative, it can be written as

$$T_1 = r_1 \exp(-i\omega x_0/V) \left\{ \int_0^{\infty} [1-\lambda/(1+\lambda^2)^{\frac{1}{2}}] \exp(-i\omega r_1 \lambda/V)\, d\lambda \right.$$
$$\left. + \int_0^{|u_1|} [1+\lambda/(1+\lambda^2)^{\frac{1}{2}}] \exp(i\omega r_1 \lambda/V)\, d\lambda \right\}. \tag{A 12}$$

Again, (A 10) can be used to evaluate (A 12).

$$(b)\ T_2 = r_1^2 \int_{u_1 r_1}^{\infty} \frac{\tau_1 \exp[-i\omega(\tau_1+x_0)/V]}{(\tau_1^2+r_1^2)^{\frac{5}{2}}}\, d\tau_1$$
$$= \frac{1}{r_1} \int_{u_1}^{\infty} \frac{\lambda \exp[-i\omega(\lambda r_1+x_0)/V}{(1+\lambda^2)^{\frac{5}{2}}}\, d\lambda. \tag{A 13}$$

By integration by parts, (A 13) can be reduced to

$$T_2 = \frac{1}{r_1} \exp[-i\omega x_0/V] \left\{ \frac{1}{3} \frac{\exp[-i\omega u_1 r_1/V}{(1+u_1^2)^{\frac{3}{2}}} - \tfrac{1}{3} i \frac{\omega r_1}{V} \left[\left(1-\frac{u_1}{(1+u_1^2)^{\frac{1}{2}}}\right) \exp(-i\omega u_1 r_1/V) \right.\right.$$
$$\left.\left. - i\frac{\omega r_1}{V} \int_{u_1}^{\infty} \left(1-\frac{\lambda}{(1+\lambda^2)^{\frac{1}{2}}}\right) \exp(-i\omega\lambda r_1/V)\, d\lambda \right] \right\}. \tag{A 14}$$

Using (A 10), T_2 can therefore be evaluated. If u_1 is negative, it can be shown that

$$T_2 = \frac{\exp(-i\omega x_0/V)}{r_1} \left\{ 2i \operatorname{Im} \int_0^{\infty} \frac{\lambda \exp(-i\omega\lambda r_1/V)}{(1+\lambda^2)^{\frac{5}{2}}}\, d\lambda \right.$$
$$\left. + \operatorname{Re} \int_{|u_1|}^{\infty} \frac{\lambda \exp(-i\omega\lambda r_1/V)}{(1+\lambda^2)^{\frac{5}{2}}}\, d\lambda - i \operatorname{Im} \int_{|u_1|}^{\infty} \frac{\lambda \exp(-i\omega\lambda r_1/V)}{(1+\lambda^2)^{\frac{5}{2}}}\, d\lambda \right\}, \tag{A 15}$$

where Im and Re stand for imaginary and real parts, respectively.

$$(c)\ T_3 = \int_{u_1 r_1}^{\infty} \frac{\tau_1 \exp[-i\omega(\tau_1+x_0)/V]}{(\tau_1^2+r_1^2)^{\frac{3}{2}}}\, d\tau_1$$
$$= \frac{\exp(-i\omega x_0/V)}{r_1} \int_{u_1}^{\infty} \frac{\lambda \exp(-i\omega\lambda r_1/V)}{(1+\lambda^2)^{\frac{3}{2}}}\, d\lambda. \tag{A 16}$$

Integrating by parts, (A 16) can be reduced to

$$T_3 = \frac{\exp(-i\omega x_0/V)}{r_1} \left\{ u_1 \left[1-\frac{u_1}{(1+u_1^2)^{\frac{1}{2}}}\right] \exp(-i\omega u_1 r_1/V) \right.$$
$$+ \int_{u_1}^{\infty} \left[1-\frac{\lambda}{(1+\lambda^2)^{\frac{1}{2}}}\right] \exp(-i\omega\lambda r_1/V)\, d\lambda$$
$$\left. - i\frac{\omega}{V} r_1 \int_{u_1}^{\infty} \lambda \left[1-\frac{\lambda}{(1+\lambda^2)^{\frac{1}{2}}}\right] \exp(-i\omega\lambda r_1/V)\, d\lambda \right\}. \tag{A 17}$$

Equation (A 17) can be directly evaluated, using (A 10). If u_1 is negative, an expression similar to (A 15) can be obtained. However, another form can be derived in the following way:

$$T_3 r_1 \exp(i\omega x_0/V) = \int_{-|u_1|}^{\infty} \frac{\lambda \exp(-i\omega\lambda r_1/V)}{(1+\lambda^2)^{\frac{3}{2}}} d\lambda$$
$$= \left\{\int_{-\infty}^{\infty} - \int_{-\infty}^{-|u_1|}\right\} \frac{(\lambda \exp(-i\omega\lambda r_1/V)}{(1+\lambda^2)^{\frac{3}{2}}} d\lambda.$$

Integrating by parts, the first term can be shown to be

$$\int_{-\infty}^{\infty} \frac{\lambda \exp(-i\omega\lambda r_1/V)}{(1+\lambda^2)^{\frac{3}{2}}} d\lambda = -2i\frac{\omega}{V}\int_0^{\infty} \frac{\cos(\omega\lambda r_1/V)}{(1+\lambda^2)^{\frac{1}{2}}} d\lambda = -2i\frac{\omega}{V} K_0\left(\frac{\omega r_1}{V}\right), \quad \text{(A 18)}$$

where K_0 is the modified Bessel function of zero order. It follows that, for negative u_1,

$$T_3 = \frac{\exp(-i\omega x_0/V)}{r_1}\left\{-2i\frac{\omega}{V} K_0\left(\frac{\omega r_1}{V}\right) + \mathrm{Re}\int_{|u_1|}^{\infty} \frac{\lambda \exp(-i\omega\lambda r_1/V)}{(1+\lambda^2)^{\frac{3}{2}}} d\lambda \right.$$
$$\left. - i\,\mathrm{Im}\int_{|u_1|}^{\infty} \frac{\lambda \exp(-i\omega\lambda r_1/V)}{(1+\lambda^2)^{\frac{3}{2}}} d\lambda\right\}. \quad \text{(A 19)}$$

Another problem in the normal-velocity evaluation is the integration involved in W_2 and W_3. In the present computer program, these integrals are evaluated by approximating the integrand by a quadratic function of τ, except for the factor $(\eta - y)/[(\eta-y)^2+z^2]$, or its variants, which are retained without approximation. The resulting expressions are then integrated exactly.

Appendix B. Mean leading-edge thrust in oscillating motion

According to the procedure used in the QVLM, the leading-edge thrust coefficient can be obtained by calculating the leading-edge singularity parameter C_s defined as

$$C_s = \lim_{x\to x_l} 2u(x)[x-x_l)/c]^{\frac{1}{2}}. \quad \text{(B 1)}$$

It should be noted that C_s will appear from those terms in the normal-velocity expressions which have Cauchy singularity in the chordwise integrals, that is, with the factor $1/Q$ when $z = 0$, where

$$Q = (x_2-x_1)(y-y_1) - (x-x_1)(y_2-y_1). \quad \text{(B 2)}$$

From appendix A, the term with $1/Q$ is seen to appear in (A 2) and is given by

$$D_1(x,y,\xi) = \frac{1}{Q}\left\{\frac{(x_2-x)(x_2-x_1)+(y_2-y_1)(y_2-y)}{[(x-x_2)^2+(y-y_2)^2]^{\frac{1}{2}}}\right.$$
$$\left. - \frac{(x_1-x)(x_2-x_1)+(y_2-y_1)(y_1-y)}{[(x-x_1)^2+(y-y_1)^2]^{\frac{1}{2}}}\right\}. \quad \text{(B 3)}$$

If the remaining normal-velocity terms in (A 1) and (A 3) are denoted by $D_0(x, y, \xi)$, the flow tangency condition from (2.3) and (2.20) becomes

$$\Sigma \int_{x_l}^{x_t} \frac{\Delta C_p(\xi)}{8\pi}[D_0(x,y,\xi)+D_1(x,y,\xi)]\,d\xi = w(x,y). \quad \text{(B 4)}$$

Again, the co-ordinate transformation (2.21) is applied and the resulting integral involving D_0 can be reduced directly to a finite sum through the midpoint trapezoidal rule. However, D_1 has Cauchy singularity because Q will vanish for some ξ for control points within the horseshoe vortex under consideration. This integral will be treated as follows (see Lan 1974).

Let

$$D(x, y, \xi) = D_1(x, y, \xi)\, Q. \tag{B 5}$$

From the co-ordinate transformation, it can be shown that

$$Q = \tfrac{1}{2}(y_2 - y_1)(\cos\theta - \cos\theta')\, c, \tag{B 6}$$

where θ' is associated with ξ and θ with x, and c is the chord length through the control points inside the vortex strip. It follows that

$$\begin{aligned} P &= \int_{x_l}^{x_t} \frac{\Delta C_p(\xi)}{8\pi} D_1(x, y, \xi)\, d\xi = \frac{1}{8\pi}\int_0^\pi \frac{\Delta C_p(\theta')\, D(x, y, \theta') \sin\theta'\, d\theta'}{(y_2 - y_1)(\cos\theta - \cos\theta')} \\ &= \frac{1}{8\pi}\int_0^\pi \frac{\Delta C_p(\theta')\, D(x, y, \theta') \sin\theta' - \Delta C_p(\theta)\, D(x, y, \theta)\sin\theta}{(y_2 - y_1)(\cos\theta - \cos\theta')}\, d\theta' \\ &\cong \frac{1}{8N_c}\sum_{k=1}^{N_c} \frac{\Delta C_p(\theta_k)\sin\theta_k\, D(\theta_k) - \Delta C_p(\theta)\sin\theta D(\theta)}{(y_2 - y_1)(\cos\theta - \cos\theta_k)}. \end{aligned} \tag{B 7}$$

It was shown that if the control points are chosen such that

$$\theta = \theta_i = i\pi/N_c, \quad i = 1, \ldots, N_c \tag{B 8}$$

and the integration points such that

$$\theta_k = (2k-1)\pi/2N_c, \quad k = 1, \ldots, N_c \tag{B 9}$$

then

$$\sum_{k=1}^{N_c} 1/(\cos\theta_i - \cos\theta_k) = 0. \tag{B 10}$$

On the other hand, if $\theta = 0$, i.e. at the wing leading edge, then

$$\sum_{k=1}^{N_c} 1/(\cos\theta - \cos\theta_k) = N_c^2, \quad \theta = 0. \tag{B 11}$$

In addition,

$$\lim_{\theta\to 0} \Delta C_p(\theta)\sin\theta = \lim_{x\to x_l} 4u(x) \times 2[(x - x_l)/c]^{\frac{1}{2}}\,[1 - (x - x_l)/c]^{\frac{1}{2}} = 4C_s \tag{B 12}$$

and

$$\lim_{\theta\to 0} \frac{D(\theta)}{y_2 - y_1} = H_s = 2(\tan^2\Lambda_l + 1)^{\frac{1}{2}}, \tag{B 13}$$

where x_l is the x co-ordinate of the leading-edge control point inside the strip which is defined by (x_1, y_1) and (x_2, y_2) at the leading edge. Λ_l is the leading-edge sweep angle. It follows that (B 7) becomes

$$P = \frac{1}{8N_c}\sum_{k=1}^{N_c} \frac{\Delta C_p(\theta_k)\sin\theta_k\, D(\theta_k)}{(y_2 - y_1)(\cos\theta - \cos\theta_k)} - \tfrac{1}{2}N_c C_s H_s, \quad \theta = 0. \tag{B 14}$$

Note that the first term in (B 14) is nothing but the upwash contributed by D_1 in (B 4). Therefore, C_s can be obtained from the following:

$$\tfrac{1}{2}N_c C_s H_s = \Sigma\,(\text{upwash at leading edge}) - w(x_l, y_l). \tag{B 15}$$

The computed C_s is a complex number in general. In applications, the real part of $C_s e^{i\omega t}$ must be taken and then time-averaged to give

$$\bar{C}_s^2 = \tfrac{1}{2}(C_{sr}^2 + C_{si}^2). \tag{B 16}$$

The mean sectional leading-edge thrust coefficient is then given by

$$c_t = \pi \bar{C}_s^2/(2\cos\Lambda_l). \tag{B 17}$$

REFERENCES

ALBANO, E. & RODDEN, W. P. 1969 *A.I.A.A. J.* **7**, 279, 2169.

BENNETT, A. G. 1970 Ph.D. thesis, University of Illinois.

BOSCH, H. 1972 Diplom-Ingenieur Thesis, Technical University, Munich.

CHADWICK, L. E. 1940 *Bull. Brooklyn Entomological Soc.* **35**, 109.

CHOPRA, M. G. 1974 *Swimming and Flying in Nature*, vol. 2 (ed. T. Y. Wu *et al.*), p. 635. Plenum Press.

CHOPRA, M. G. & KAMBE, T. 1977 *J. Fluid Mech.* **79**, 49.

DAVIES, D. E. 1963 *Aero. Res. Counc. R. & M.* no. 3409.

HERTEL, H. 1966 *Structure-Form-Movement.* New York: Reinhold.

JORDAN, P. F. 1976 *Z. Flugwiss.* **24**, 205.

KÁLMÁN, T. P., GIESING, J. P. & RODDEN, W. P. 1970 *J. Aircraft* **7**, 574.

LAN, C. E. 1974 *J. Aircraft* **11**, 518.

LAN, C. E. 1975 *Univer. Kansas Center Res. Inc., Lawrence, Kansas, Tech. Rep.* KU–FRL–400.

LAN, C. E. 1976 *N.A.S.A.* SP–405, paper no. 21.

LAN, C. E. & LAMAR, J. E. 1977 *N.A.S.A. Tech. Note* D–8513.

LASCHKA, B. 1975 *AGARD*–R–645.

LIGHTHILL, M. J. 1970 *J. Fluid Mech.* **44**, 265.

PRINGLE, J. W. S. 1957 *Insect Flight.* Cambridge University Press.

RICHARDSON, J. R. 1955 *Aero Res. Counc. R. & M.* no. 3157.

SPARENBERG, J. A. & WIERSMA, A. K. 1974 *Swimming and Flying in Nature*, vol. 2 (ed. T. Y. Wu *et al.*), p. 891. Plenum Press.

STAHL, B., KÁLMÁN, T. P., GIESING, J. P. & RODDEN, W. P. 1968 *Douglas Aircraft Co., U.S.A. Rep.* DAC–67201.

WU, T. Y. 1971 *J. Fluid Mech.* **46**, 521.

WU, T. Y. 1972 *J. Ship Res.* **14**, 66.